Supporting Information
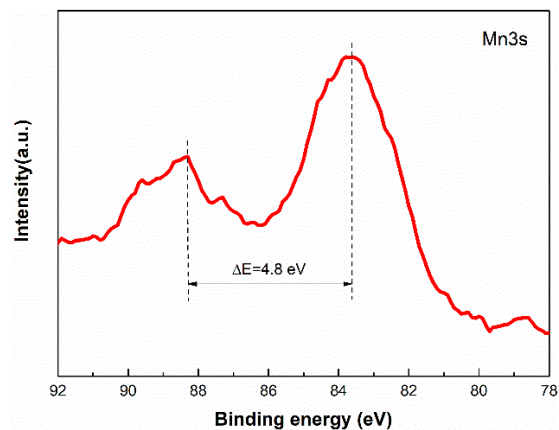
Xiaole Zhang, Song Li*, Shenghe Wang, Zhenxu Wang, Zhongsheng Wen, Shijun Ji,

Juncai Sun
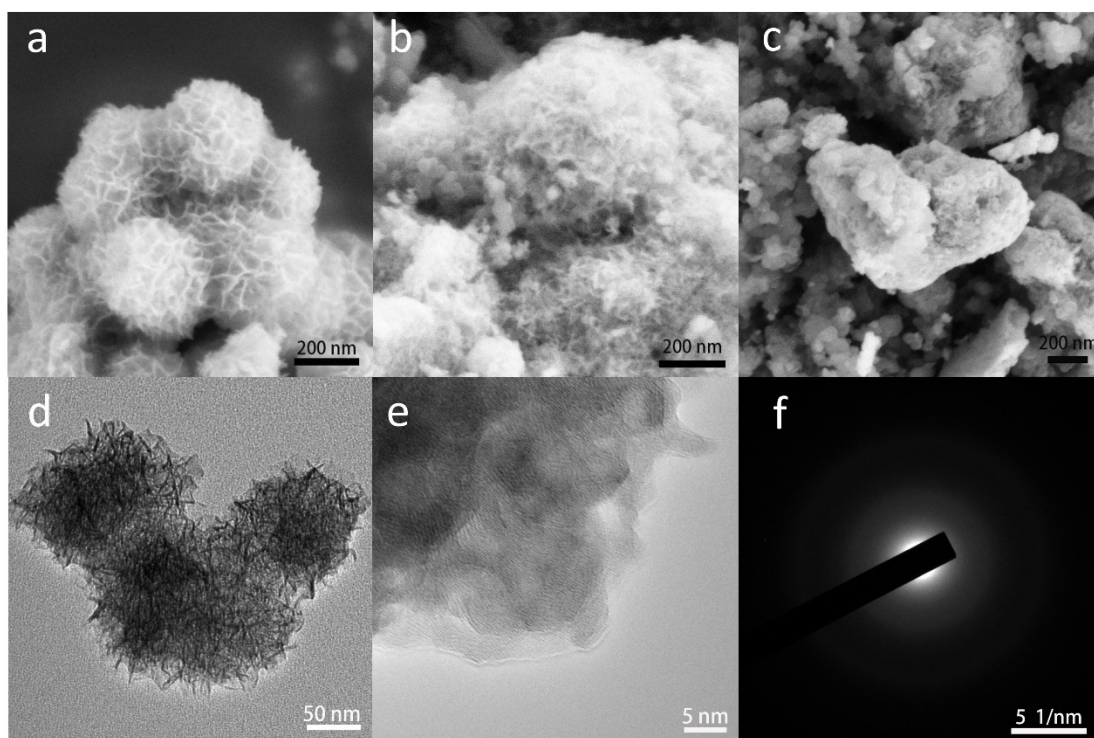
Institute of Materials and Technology, Dalian Maritime University, Dalian 116026,

China

*Corresponding author. E-mail: lisong@dlmu.edu.cn (S Li).

Fig. S1. High-resolution Mn 3s of a-MnO$_2$/AB.

Fig. S2. SEM images of (a) a-MnO$_2$, (b) a-MnO$_2$/AB and (c) a-MnO$_2$-500/AB, (d)TEM and (e)

HRTEM images and corresponding SEAD pattern (f) of a-MnO$_2$/AB.

As shown in **Fig. S2**, a-MnO$_2$ nanosheets are interlinked to form a hierarchical porous sphere.

The HRTEM image of a-MnO$_2$ exhibits no observable lattice fringing, confirming the present of

amorphous phase. Furthermore, the selected area diffraction (SAED) of a-MnO$_2$/AB shows faint

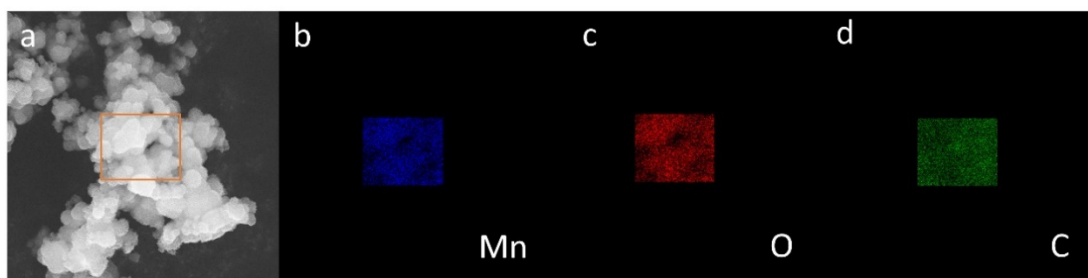diffraction rings due to the amorphous nature.

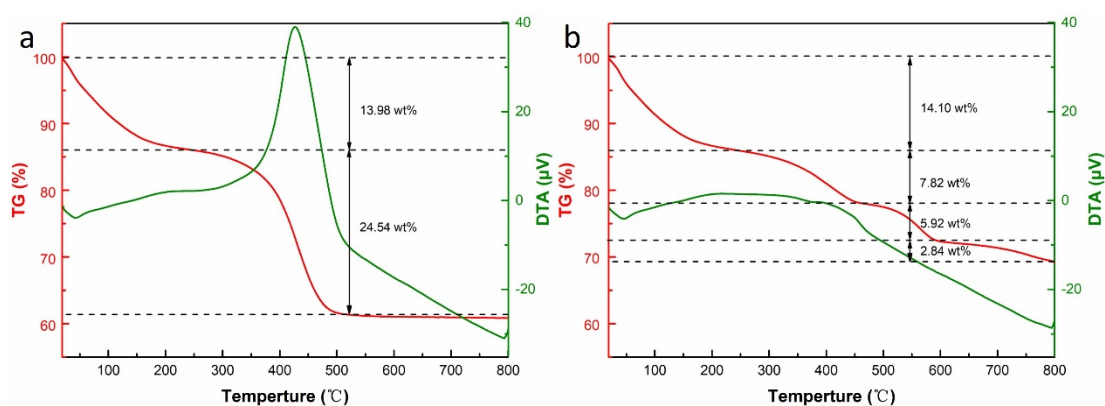Fig. S3. EDS mappings of Mn, O and C in a-MnO$_2$/AB.

Fig. S4. TGA results under air (a) and N$_2$ (b) conditions for a-MnO$_2$/AB.

The weight loss from room temperature to 250 °C under air is associated with the evaporation of water, and the apparent mass reduction between 250 °C and 500 °C is due to the complete oxidation of AB. The results indicate that the percentage of AB in a-MnO$_2$/AB composite is 24.54 wt%. In addition, the weight loss is negligible from 500 °C to 800 °C. In contrast, the weight loss from room temperature to 250 °C in N$_2$ was similar to that in air. The decrease in weight loss (7.82 wt%) in the range of 250 °C ~ 470 °C is mainly due to the incomplete oxidation of AB in N$_2$, indicating some amount of AB can be retained after the heat treatment in N$_2$. There are still weight loss of 5.92 wt% and 2.84 wt% between 500 °C and 800 °C, which may be related to the continuous loss of oxygen of MnO$_2$ in N$_2$. It demonstrates that the MnO$_2$ is more prone to oxygen loss in N$_2$. Therefore, the heat treatment temperature for

obtaining crystalline MnO_2 is adopted at 500 °C.

Table S1. BET surface area and porosity of a-MnO_2/AB and a-MnO_2-500/AB samples.

Sample	BET surface area (m²/g)	Pore volume (cm³/g)	Pore width (nm)
a-MnO_2/AB	165.95	0.28	6.788
a-MnO_2-500/AB	146.38	0.27	7.388
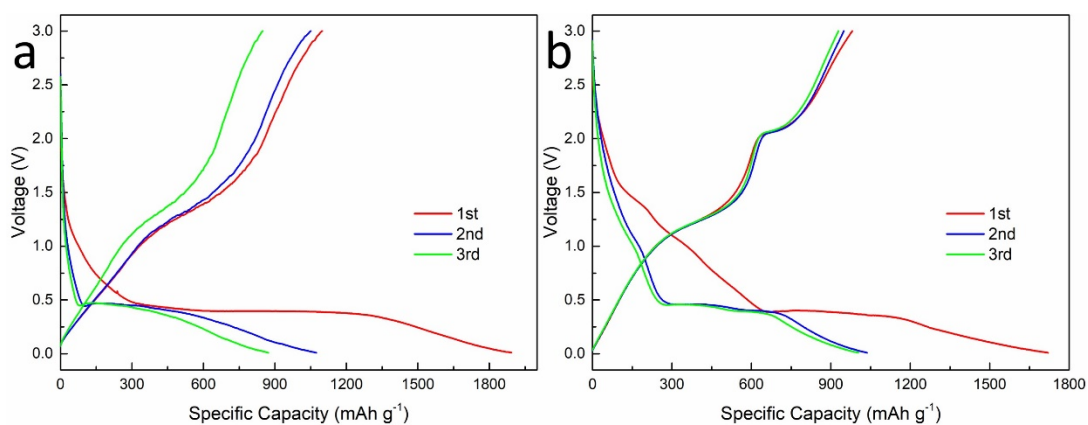
Fig. S5. Galvanostatic discharge/charge curves of a-MnO_2 and a-MnO_2-500/AB at 0.1A g⁻¹.

Table S2. A summary of the electrochemical performance of the a-MnO_2/AB sample and other oxide/carbon materials.

Materials	Initial coulomb efficiency	Reversible capacity (mAh g⁻¹) [C-rate A g⁻¹]	Capacity retention (mAh g⁻¹) (after n cycles) [C-rate A g⁻¹]	Ref.
Amorphous MnO_2	-	180 [1.6]	530 (n=50) [0.1]	[14]
Amorphous MnO_2/RGO	53.0%	295 [2]	784 (n=500) [1]	[21]
MnO_2@TiO_2	86.0%	87 [6]	938 (n=200) [0.3]	[3]

β-MnO$_2$/RGO	50.5%	159 [1]	420 (n=50) [0.1]	[18]
NiO@MnO$_2$	75.8%	787 [5]	1000 (n=160) [1]	[32]
MnO$_2$@Fe$_3$O$_4$/CNT	58.0%	300 [10]	873 (n=500) [2]	[33]
3D δ-MnO$_2$	72.0%	135 [2]	1150 (n=200) [1]	[45]
SnS$_2$/C	-	150 [1]	428 (n=50) [1]	[34]
SiO$_2$/Fe$_3$O$_4$/C	62.7%	50 [1.6]	140 (n=100) [0.1]	[35]
Fe$_2$O$_3$/Mn$_2$O$_3$	62.0%	435 [2]	400 (n=500) [1]	[37]
a-MnO$_2$/AB	72.3%	318 [9.6]	1300 (n=300) [1]	This work

Table S3. The R$_{ct}$ of the a-MnO$_2$/AB and a-MnO$_2$-500/AB samples.

Sample	After 1 cycle R$_{(sf+ct)}$/Ω	After 5 cycle R$_{(sf+ct)}$/Ω	After 10 cycle R$_{(sf+ct)}$/Ω	After 50 cycle R$_{(sf+ct)}$/Ω	After 100 cycle R$_{(sf+ct)}$/Ω	After 200 cycle R$_{(sf+ct)}$/Ω
a-MnO$_2$/AB	37.16	22.05	32.04	31.55	28.13	30.30
a-MnO$_2$-500/AB	38.44	42.21	69.24	102.01	237.86	462.19
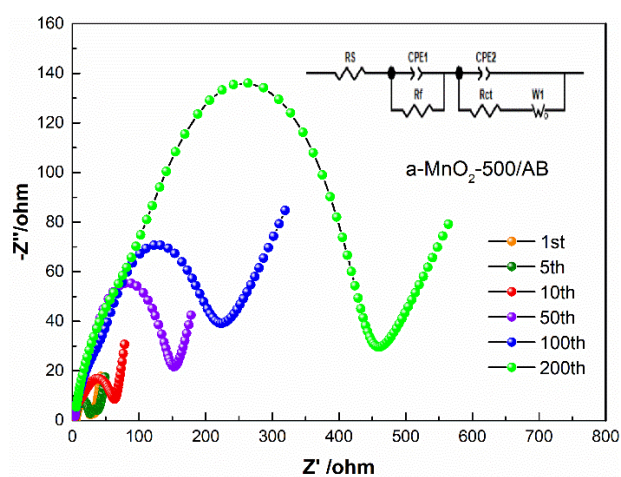
Fig. S6. Impedance measurements of a-MnO$_2$-500/AB after 1st, 5th, 10th, 50th, 100th and 200th cycle at 1 A g^{-1}.

The reaction kinetics of the a-MnO$_2$/AB electrode were further explored in detail by CV measurements. The relationship between the current (i) and the sweep rate (v), as shown in the following equation: [1]

$$i = av^b \qquad (1)$$

Where a and b are two changeable parameters. It is well-known that b-value of 0.5 means total diffusion control behavior and b-value of 1 indicates capacitive process. [2] In addition, the capacity contribution from capacitive and diffusion-controlled charge can be calculated on the basis of the relationship:

$$i = k_1 v + k_2 v^{1/2} \qquad (2)$$

Where $k_1 v$ and $k_2 v^{1/2}$ represent the capacitive process and diffusion-controlled process, respectively.
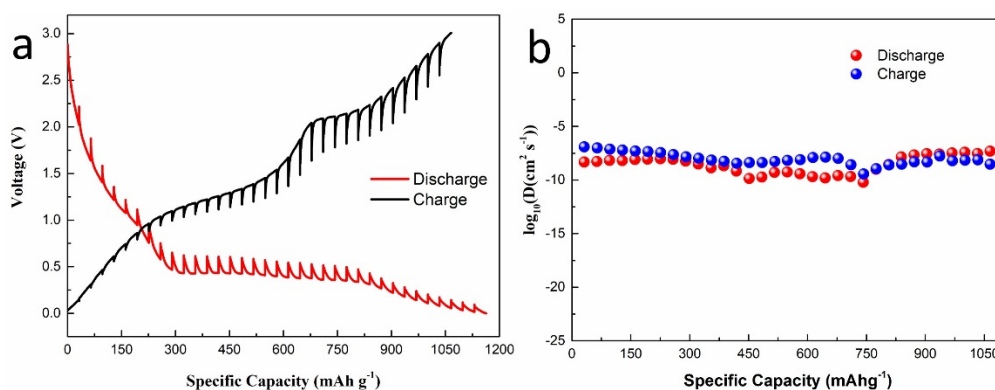
Fig. S7. (a) GITT curves and (b) corresponding D_{Li}^+ diffusion coefficients of

a-MnO$_2$-500/AB electrodes.

The lithium-ion diffusion coefficient (D_{Li}^+) is calculated GITT (Fig. S6) according to the following equations: [3]

$$D_{Li+} = \frac{4}{\pi \tau} \left(\frac{m_B V_M}{M_B S} \right)^2 \left(\frac{\Delta E_S}{\Delta E_\tau} \right)^2 \qquad (3)$$

Where m_B, V_M and M_B are the active mass loading, molar volume and molar mass, respectively, S is the area of the electrode-electrolyte interface, τ is the constant current pulse duration and $\Delta E\tau$ is the total change in the battery voltage during a constant current pulse τ. ΔE_S is the change in steady-state voltage during constant current titration.

References

1.   X. Liu, X. Zhang, S. Ma, S. Tong, X. Han and H. Wang, *Electrochimica Acta*, 2020, **333**, 135568.

2.   K. Liu, J.a. Wang, J. Yang, D. Zhao, P. Chen, J. Man, X. Yu, Z. Wen and J. Sun, *Chemical Engineering Journal*, 2021, **407**, 127190.

3.   M. Liao, J. Wang, L. Ye, H. Sun, Y. Wen, C. Wang, X. Sun, B. Wang and H. Peng, *Angew Chem Int Ed Engl*, 2020, **59**, 2273-2278.